RMetS
Royal Meteorological Society

The February 2010 Arctic Oscillation Index and its stratospheric connection

P. Ripesi,[a]* F. Ciciulla,[b] F. Maimone[b] and V. Pelino[b]

[a]*Department of Physics and INFN, University of Rome Tor Vergata, Rome, Italy*
[b]*Italian Air Force, CNMCA, Aeroporto De Bernardi, Pratica di Mare, Rome, Italy*

*Correspondence to: P. Ripesi, Dept. of Physics, University of Tor Vergata, Via della Ricerca Scientifica 1, 00133 Roma, Italy. E-mail: patrizio.ripesi@roma2.infn.it

The atmospheric dynamics during the occurrence of the extreme negative value of the Arctic Oscillation Index in February 2010 are investigated using meteorological fields from ERA-Interim and ERA-40 reanalysis data. The study focuses on the possible causes of this anomalous value, finding that it was forced by a geopotential anomaly that propagated downward from the stratosphere to the troposphere in association with a major sudden stratospheric warming event which occurred at the end of January. An analysis of the dynamics of this warming is also developed, together with a comparison with past similar events. Synoptic and spectral properties of the geopotential fields are analyzed, and the time series of the 'Baroclinic Activity Index' are computed, finding an abrupt increase of the middle latitude baroclinic activity immediately after the central date of the warming event. A possible interpretation of this feature is proposed.

Key Words: hemispheric teleconnections; sudden stratospheric warmings; baroclinic activity index

Received 16 June 2011; Revised 23 February 2012; Accepted 5 March 2012; Published online in Wiley Online Library

Citation: Ripesi P, Ciciulla F, Maimone F, Pelino V. 2012. The February 2010 Arctic Oscillation Index and its stratospheric connection. *Q. J. R. Meteorol. Soc.* DOI:10.1002/qj.1935

1. Introduction

The Arctic Oscillation Index (AOI) is one of the most prominent indices describing a major variability mode of the atmosphere in the Northern Hemisphere (NH). Its modulations are closely linked to the intensity of the NH polar vortex: a positive value of the AOI is associated with a strong vortex, while a negative one denotes a weak vortex (Thompson and Wallace, 1998). The AOI is also found to be highly correlated with the tropospheric circulation, meaning that during a positive phase of AO, the hemispheric circulation is predominantly zonal, while during a period of negative AOI the meridional flux of air masses is enhanced.

Recent studies (Baldwin and Dunkerton, 1999, 2001; Christiansen, 2001) have shown that some mid-stratospheric anomalies, such as geopotential and temperature anomalies, can propagate downward to the troposphere after the occurrence of sudden stratospheric warming (SSW) events (on a time-scale of order of weeks). These anomalies have been found to influence the tropospheric state through a number of possible mechanisms, including the descent of the critical lines (Matsuno, 1971), potential vorticity inversion (Harley *et al.*, 1998) and downward reflection of planetary waves (Perlwitz and Harnik, 2003). These mechanisms affect the structure and intensity of the polar vortex itself, resulting also in a change of the tropospheric AO signal. In fact, there is a tendency for negative values of AOI after an SSW event (Limpasuvan *et al.*, 2004), in particular after those events dominated by a wave-2 geopotential component (Nakagawa and Yamazaki, 2006). Apart from the large-scale circulation impact, a statistically significant increase in the baroclinic activity in the troposphere has been noted, both from numerical studies and observations (Polvani and Kushner, 2002; Wittman *et al.*, 2007; Simpson *et al.*, 2009; Tanaka and Tokinaga, 2002).

During February 2010, the AOI reached its most negative value since 1950, i.e. since high-resolution data have become available. According to the mentioned correlation between the AOI and the tropospheric circulation, that month was characterized by a series of severe cold

weather conditions over North America (e.g. snow cover maps at http://www.nohrsc.noaa.gov/nsa/) and over Europe (http://www.dwd.de/, section 'Climate+Environment'). On the other hand, the 2009–2010 winter NH was characterized by an intense Rossby wave activity, presumably connected to the concomitant occurrence of an El Niño phenomenon of moderate to strong intensity, whose upward propagation repeatedly disturbed the polar vortex from early November 2009 to the end of February 2010.

In the present work we have analyzed the causes of the extreme value reached by the AOI in February 2010. In section 2 we briefly describe the data and the analysis methods used. In section 3 we examine the stratospheric and tropospheric dynamics for the period January–February, with a focus on the synoptic and spectral features of the fields. Section 4 contains a comparison with the events observed in the past. Then, in section 5, we give some additional discussions, while section 6 concludes the paper.

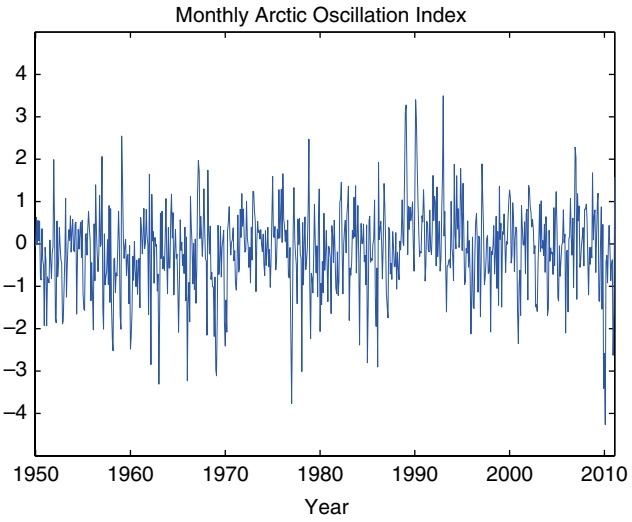

Figure 1. Monthly mean AOI, from January 1950 to April 2011. This figure is available in colour online at wileyonlinelibrary.com/journal/qj

2. Data and analyses

In this study we have used the daily mean data from the European Centre for Medium-range Weather Forecasts (ECMWF) reanalysis datasets ERA-Interim and ERA-40 with 2.5° latitude by 2.5° longitude resolution over a total of 22 pressure levels from 1000 to 1 hPa. A detailed study of the event was made for January–February 2010, while the months from December to April of the years 1958 to 2009 were used for climatological comparison. Monthly and daily mean AOI at 1000 hPa has been retrieved from the (US) National Oceanographic and Atmospheric Administration (NOAA) web site (http://www.cpc.ncep.noaa.gov).

As a main diagnostic tool for the wave activity, we used the Eliassen–Palm (E–P) flux (Eliassen and Palm, 1961; Palmer, 1982), while to explore the contributions of the various geopotential zonal wave numbers to the tropospheric forcing, we performed a Fourier analysis of the geopotential field.

Following Benzi (1986), Hansen and Sutera (1986) and Vitolo *et al.* (2009), we computed the time series of the Baroclinic Activity Index (BAI) and used it as a proxy for the baroclinc activity in the middle latitudes. The BAI was calculated by taking the geopotential height field at 500 hPa and averaging it over the latitudinal band 30°–60°N. After a Fourier decomposition of this quantity, BAI is defined as the mean square root of the sum of wave numbers 6–8. In the same way, we have defined an ultra-short synoptic wave index (which we will refer to as BAI_2) for the wave numbers 9–11, which we used to put into context the timing of the tropospheric response in different synoptic wavelength ranges.

3. Results

The 2009–2010 winter NH was characterized by a series of extremely low mean monthly AOI, starting in December (Wang and Chen, 2010) and culminating with the negative peak of February, when the AOI reached the record value of −4.266. The historical time series of monthly mean AOI, from 1950 to 2011, is shown in Figure 1.

In order to get a closer look at this anomalous condition, let us consider the AOI daily evolution from 1 January to 28 February 2010 (Figure 2(a)). From this time series, we can see that, after an initial negative peak in the first days of January, the index rose until the middle of the month and then dropped to strong negative values, which lasted through February.

Analyzing the atmospheric pattern of the same period, we find that the initial (i.e. at the beginning of January) AOI negative values were due to a residual tropospheric geopotential anomaly associated with a minor SSW event, which occurred during the first half of December. This anomaly consisted of blocking configurations over the upper Atlantic and Pacific Oceans which affected only the lower stratospheric structure of the polar vortex, while leaving its upper stratospheric part almost unchanged.

The subsequent (late January) AOI negative value, in contrast, was due to a new geopotential and temperature anomaly, formed on 20 January, which propagated downward from the stratosphere to the troposphere, affecting the whole polar vortex structure. The latter anomaly reached its maximum value on 12 February around 200 hPa, as shown in Figure 2(b, c), and was associated with a major SSW event which started from the middle of January and culminated on 27 January, the central date of SSW according to the definition in Charlton and Polvani, 2007 (Figure 2(d)).

Figures 2(d–f) show the time series of some atmospheric field averages, which can be taken, following Coy *et al.* (2009), as indicators of the stratospheric response to the tropospheric forcing. As we can see, the 10 hPa eddy momentum flux ($\overline{u'v'}$), zonally averaged at 50°N, gradually rose until the end of January, together with the eddy heat flux ($\overline{v'T'}$) (not shown). This latter resulted in a growth of the polar stratospheric temperature of about 40 K in a week, which induced a complete reversal of the meridional temperature gradient and caused the change of the zonal wind direction from westerly to easterly. Under the effect of forcing, the polar vortex was weakened, shifted out from the pole and split into daughter vortices.

Following the dynamics of the polar vortex during January–February, i.e. looking at the geopotential and potential vorticity fields, this period can be divided into three main stages of development:

(i) a displacement phase, from 15 January to 28 January;
(ii) a first split phase, from 28 January to 8 February;
(iii) a second split phase, from 8 February to 28 February.

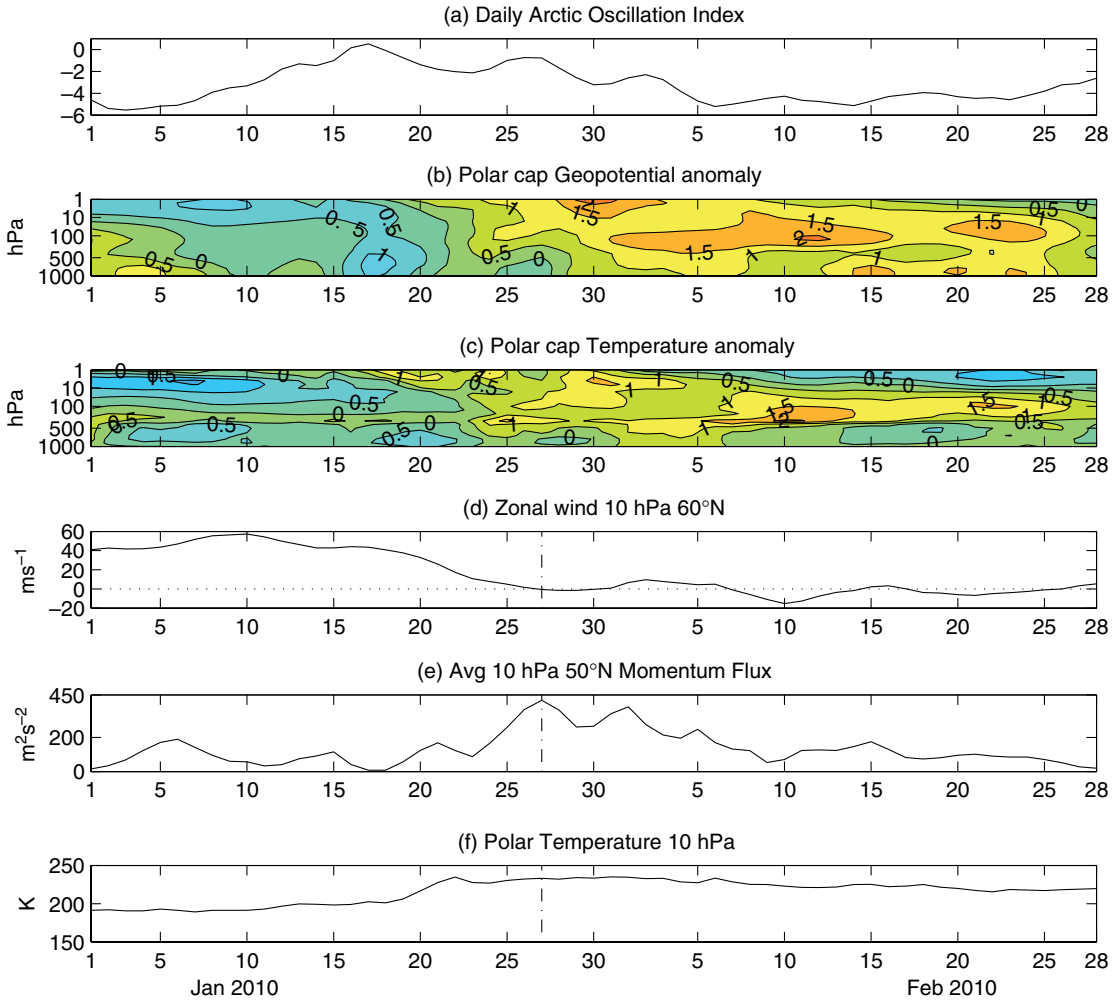

Figure 2. Time evolution, from 1 January to 28 February 2010, of (a) daily mean AOI; (b) normalized 1000–1 hPa geopotential height anomaly with respect to its climatological average (1989–2009), averaged poleward of 60°N; (c) is as (b), but for the temperature anomaly; (d) 10 hPa 60°N zonally averaged zonal wind ($m\,s^{-1}$); (e) 10 hPa 50°N zonally averaged momentum flux (m^2s^{-2}); and (f) 10 hPa 90°N temperature (K). The vertical dash-dotted line denotes the central date, corresponding to the first day with negative zonal wind. The dotted line in (d) marks the zero axis. This figure is available in colour online at wileyonlinelibrary.com/journal/qj

Before going on with the description of each phase, it is worthwhile to note that this separation could also be inferred quantitatively, for example by means of the method of geometric moments developed by Hannachi *et al.* (2011). However, as stated in the section devoted to climatology, our case presents no particular ambiguities, if compared with the commonly quite elusive timing of the phenomenon.

3.1. *Displacement*

The displacement phase coincides with the first steps of the warming event, and spanned the time period from the middle of January to 28 January. As we can see in Figure 3, the dominant 10 hPa geopotential (zonal) wave component during this period is number 1; looking at Figure 4, showing the northern hemisphere 10 hPa geopotential field, we find that this strong wave component was associated with an extensive anticyclonic circulation centred over the Aleutian Islands, which propagated from the troposphere to the stratosphere. This ridge, present since the early days of the month, intensified from 15 January onwards, and forced the polar vortex to shift over Eurasia (as shown in the sequence of Figure 4); its appearance was also locally associated with a great enhancement of the 10 hPa heat and momentum eddy fluxes, ($v'T'$) and ($u'v'$) respectively (not shown).

With reference to Figure 5, showing the E–P fluxes and the zonal wind vertical sections for some days together with their January climatological averages, we can see that the E–P flux components on 21 and 26 January were strong compared to their climatological values. This is indicative of an intense wave activity which, during the days before the central date, entered into the stratosphere from the troposphere, disturbing the stratospheric circulation from the middle to polar latitudes. Looking at the zonal wind, we find that the first easterly currents started on 21 January poleward of 80°N and propagated downward and southward following the convergence zone of the E–P flux, according to the non-acceleration theorem (Charney and Drazin, 1961; Andrews *et al.*, 1987, pp.130–133).

3.2. *First split*

After the peak-event of 24 January, associated with the mentioned anticyclonic circulation, the amplitude of the geopotential wavenumber 1 component started to drop, while wavenumber 2 component abruptly increased beyond 28 January (Figure 3). This event was due to the formation

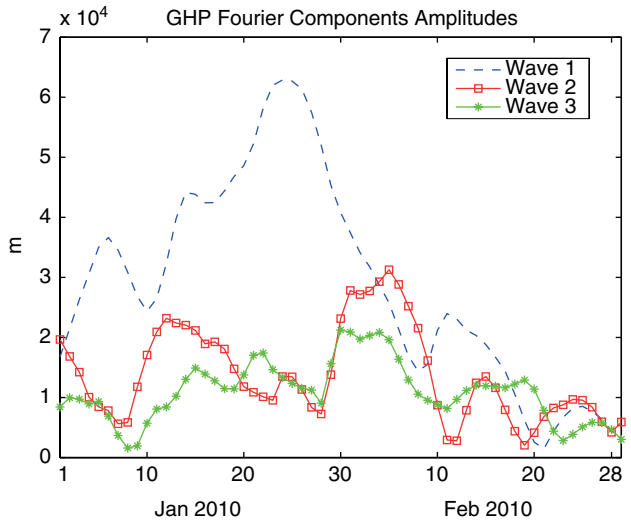

Figure 3. Time series of the 10 hPa 30–60°N averaged geopotential height wave components: 1 (dashed line), 2 (line with squares) and 3 (line with asterisks) from 1 January to 28 February 2010. This figure is available in colour online at wileyonlinelibrary.com/journal/qj

of a new anticyclonic system, centred over Eurasia, which propagated to the stratosphere and forced the polar vortex until its breaking on 4 February. From the 10 hPa geopotential height field evolution, we can see that during this day the polar vortex was split into two distinct centres located over northern Europe and over central China, with the former presenting a wider spatial extension and the latter vanishing a few days later (Figure 4). This behaviour is in agreement with well-known results (e.g. Andrews *et al.*, 1987; Martius *et al.*, 2009, provide a more recent review), according to which the geopotential wavenumber 1 component causes the displacement of the polar vortex, while wavenumber 2 is at the origin of the split.

The first split phase spanned the time period from 28 January to 8 February, during which a reduction of the E–P flux in the stratosphere is found, corresponding to a reduction of both momentum (Figure 2(e)) and heat eddy flux components (not shown).

A further comment is in order concerning the propagation, in the central part of this period, of the geopotential and temperature anomaly, since the latter appears not to efficiently propagate deep into the lower troposphere, unlike the former. This fact is related to the planetary-wave heat transport, which is much more efficient in the upper troposphere and above it, since the planetary wave amplitudes grow with height. Instead, in the lower troposphere, the dominant transport mechanism is driven by baroclinic waves, which guide (or inhibit) heat fluxes from lower latitudes across 60°N. As a consequence, below 500 hPa the temperature anomaly induced by planetary-wave heat transport is greatly masked. This behaviour is observed in almost any past SSW event, as will be pointed out in section 4.

3.3. *Second split*

Following the dynamics of the polar vortex, we observe that after its breakdown on 4 February, the Euro-Asiatic ridge rotated to the west, became positioned over the North Atlantic Ocean, allowing the polar vortex to recompose on the thin line connecting Northern Europe to Greenland at 60°N. Later, on 11 February, a new anticyclonic centre appeared over Eurasia and started to force the polar vortex until (on 19 February) it was split into three distinct centres of action located over Asia, Europe and Canada, with the last one having a wider spatial extent (Figure 4).

Looking at the corresponding geopotential zonal wave signal (Figure 3), we can see that the geopotential wave 1 component increased until 10 February, after which it dropped while the wave 3 component started to rise. Following these dynamics, wave component 1 became the dominant one up to 15 February; then wave 3 component started to prevail, forcing the polar vortex to break. The vortex then became weaker and distorted and remained so for the rest of the month, with the two persisting separate European and Canadian centres, while the Asian centre slowly disappeared.

As a possible physical mechanism leading to this wave-3 splitting event, it can be inferred that Rossby wave-3 upward pulse could have originated from the exceptional extension of snow cover over the Eurasian region (Cohen *et al.*, 2010), lasting from early October, with its associated cold air high pressure centre. As a matter of fact, it is interesting to note that the December–February Eurasian snow cover extent, as derived from NOAA's satellite-sensed observations (Robinson *et al.*, 1993), was the second greatest during the period 1966–2010. In spite of this, it is hard to assert how much the origin of the AOI record value was due to this anomalous snow cover; while it most probably influenced the origin of the wave-3 forcing, it is not equally true that this forcing was the dominant factor of the AOI negative peak, as we will point out in the final section.

4. Comparison with past split events

In order to put the previous analysis in context, and to assess the peculiar characteristics of the stratospheric phenomena which have preceded the extreme AOI, we made a comparison with past SSW split events. The latter have been isolated using the algorithm introduced by Charlton and Polvani (2007), based on the recognition of separate potential vorticity spots, after a previous identification of a central date, corresponding to the reversal of the zonal wind at 60°N and 10 hPa. The SSW events with central dates occurring during the first half of December and during the last half of March have been discarded in order to keep the analysis more coherent with respect to the present case-study, since early and final-type SSWs are normally associated with a relatively weak polar vortex. For the analysis, we have used an extended dataset, extracted from both ERA-40 (from 1958 to 1978) and ERA-Interim (from 1979 to 2009) reanalysis data, in order to include the most recent years. A total of twelve splitting events from 1958 to 2009 have been identified and studied, taking into account 25 days before and after the central date. Table 1 shows a list of the events, followed by the daily AOI time-averaged over the relevant intervals of $(-25, +25)$ and $(0, +25)$ days around and after the central date, respectively. We note that the 2010 historical record is maintained even considering averages over these time periods.

In Figure 6(a–c), a time–height section is reported of the mean geopotential anomaly, the mean temperature anomaly, and the mean daily AOI relating to the seven split years from 1979 to 2009. They show a clear tendency for the anomaly to be reproduced at lower and lower levels after

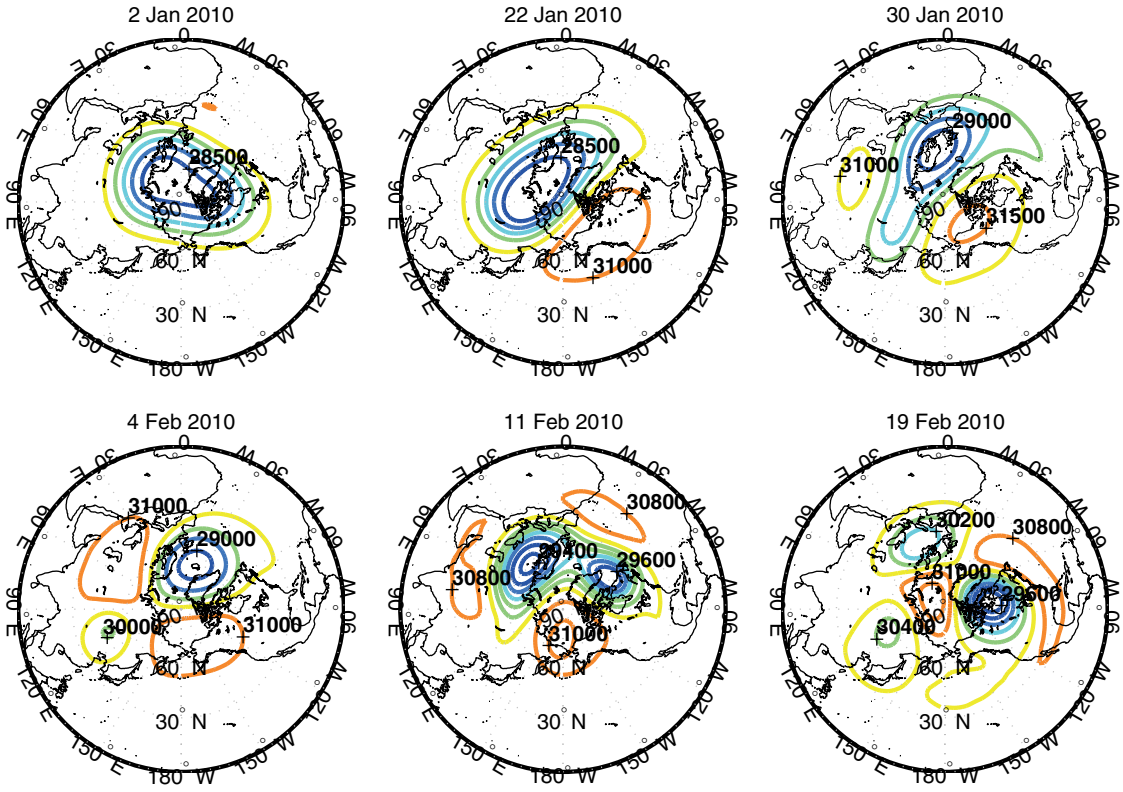

Figure 4. Maps of 10 hPa geopotential height (contour interval 200 m) for 2, 22 and 30 January, and for 4, 11, 19 February 2010. The high/low values are marked in bold. This figure is available in colour online at wileyonlinelibrary.com/journal/qj

Table 1. List of split events, with central date from 15 December to 14 March, extracted using the ERA-40 and ERA-Interim datasets. The third and fourth columns show the average AOI over the interval (–25, +25) and (0, +25) days referred to the central date, respectively.

No.	Central date	AO mean value (–25, +25)	AO mean value (0, +25)
1	31 January 1958	–1.8100	–2.0036
2	23 February 1966	–1.0491	–0.4295
3	7 January 1968	–0.3255	–0.4452
4	18 January 1971	–0.6721	–0.5144
5	31 January 1973	+0.9500	+1.0085
6	22 February 1979	–0.7991	–0.5786
7	1 January 1985	–1.2541	–3.0009
8	21 February 1989	+2.6102	+1.8729
9	26 February 1999	–0.6361	–1.7013
10	4 January 2004	–0.8564	–1.7584
11	12 March 2005	–1.4012	–0.6956
12	24 January 2009	–0.1256	–0.8450
13	27 January 2010	–3.1780	–3.7251

the central date (with the geopotential anomaly eventually arriving at the ground, and the temperature anomaly confined above 500 hPa), and for the AOI to assume, after the central date, weakly negative values, becoming even more negative about 10 days later.

The peculiar character of the present case (Figure 2) is then evident, exhibiting a separate and strong peak of the anomaly 15 days after the central event just above the troposphere. This fact is confirmed by a comparison with the previous past events (not shown), including those covering the whole ERA-40 period. The only event showing a similar geopotential and temperature anomaly pattern is the 1985 one, though it presented a lower intensity and quite different underlying dynamics.

Looking at Figure 6(d), showing the mean values of wave components 1–3 of the geopotential field, it can be seen that a typical splitting phenomenon starts with a wave-1 dominating period, followed by a wave-2 overtaking before the common decrease of both components; it appears that wave-3 forcing never prevails, even from the analysis of each past event separately.

From the latter circumstance, we can infer that one of the most peculiar features of the 2010 event is the seemingly unprecedented (in the observations) role of the wave-3 component which was, in the last stage of the phenomenon, the dominating one, and was associated with a splitting of the vorticity pattern into three separate patches.

5. Discussion

Regarding physical mechanisms guiding the observed return signal from the stratosphere back to the troposphere, we note

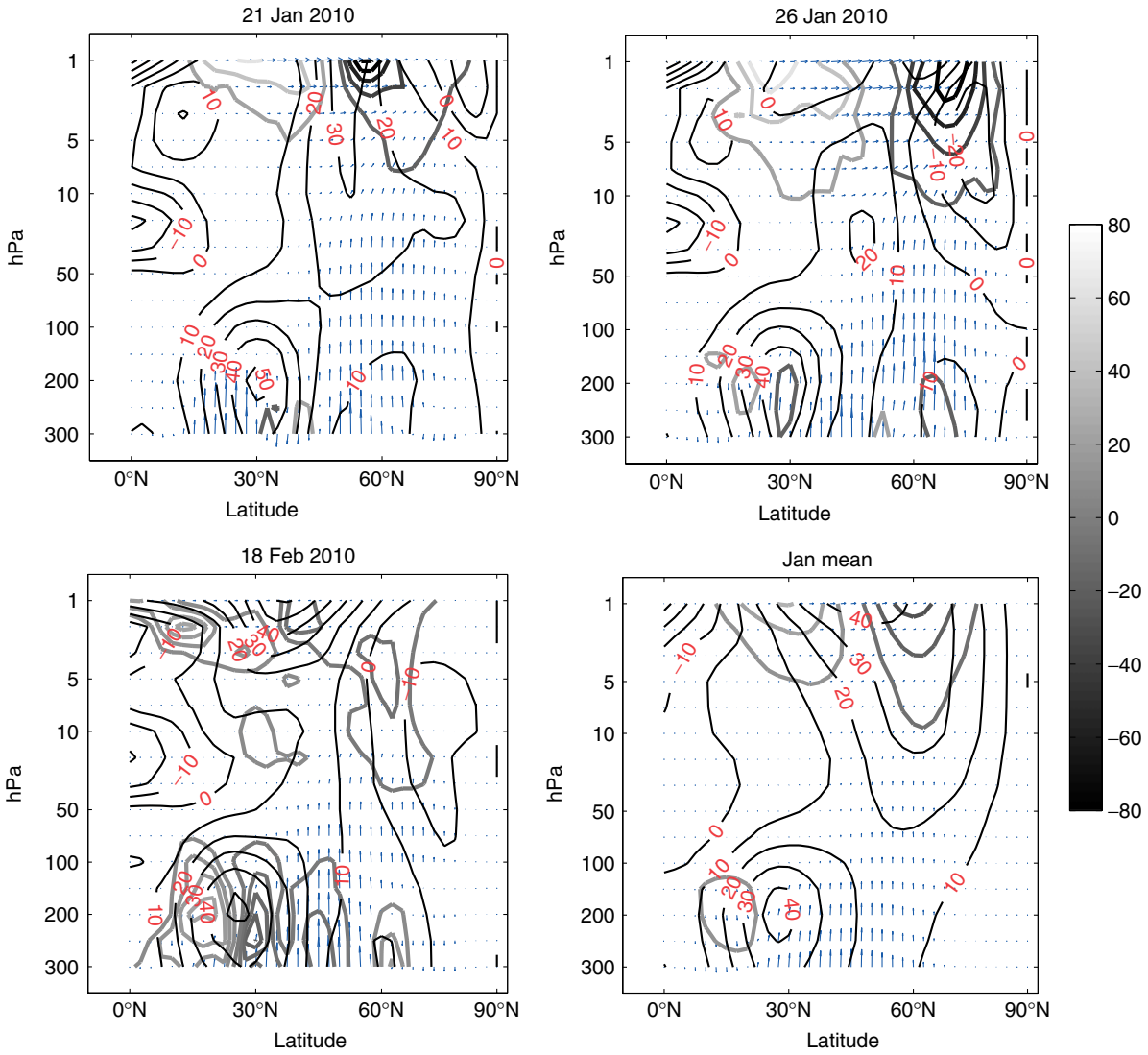

Figure 5. Vertical section of E–P flux (arrows), E–P convergence (bold lines with line shading denoting values) and of zonal wind (thin lines) for 21 and 26 January, 18 February and the 1989–2009 January climatological values. The vertical component of E–P flux has been scaled by a factor $(R/100)^{-1}$, with R the Earth radius (m), to better visualize the divergence zones. This figure is available in colour online at wileyonlinelibrary.com/journal/qj

that the most significant SSW event was followed, in our case-study, by a peak of baroclinic activity in the middle-latitude troposphere. One convenient way to quantify its growth is by using the Baroclinic Activity Index (BAI; Benzi *et al.*, 1986; Hansen and Sutera, 1986; Vitolo *et al.*, 2009), which considers wave number components 6–8, and by using the newly defined index BAI_2 for wave numbers 9–11. In fact, it has been shown that amplitudes from wavenumber 5 and larger are fed by the normal conversion from available potential energy to eddy kinetic energy (Blackmon, 1976; Speranza, 1983). Consequently, this index can be considered a good proxy for the baroclinic activity at the middle latitudes.

As is clearly visible in Figure 7(a–c), BAI reached its maximum on 25 January, while BAI_2 peaked soon after, on 26 January, following the maximum of wavenumber-1 vertically integrated energy flux (Matsuno, 1970) averaged over the latitudinal band 30°–85°N at 10 hPa, which occurred on 19 January. It should be stressed, as revealed by a further Fourier decomposition of the 500 hPa geopotential signal averaged over 30°–60°N (not shown), that all wavenumbers within BAI and BAI_2 present these distinctive peaks. Besides, with reference to the period considered, BAI and BAI_2 are observed to increase to about 10% of their mean values after the occurrence of their relative peaks. We suggest that this behaviour of the baroclinic activity is likely to be connected with the downward energy flux from the stratosphere to the troposphere, starting from 24 January. This energy flux is observed to be displaced from polar latitudes (north of 75°N) towards the middle latitudes at the end of the month, following the zones of negative zonal wind, as obtained from a direct calculation of the vertical wave-1 energy flux as a function of pressure and latitude (not shown). These latter observations, together with the above-mentioned time delay of the geopotential amplitude peaks associated with BAI and BAI_2, are indicative of a mechanism of energy transfer from the vertically trapped Rossby waves to smaller baroclinic scales.

On the other hand, middle latitude geostrophic turbulence is known to play a central role in the atmospheric mass exchange across the latitudinal circle at 60°N and hence can be considered as a secondary modulating factor of the AO (Tanaka and Tokinaga, 2002, and references therein). In this respect it is interesting to note, from a direct cross-analysis of the Tibaldi–Molteni blocking index (data available at http://icdc.zmaw.de/blocking_index.html?&L=1) and the

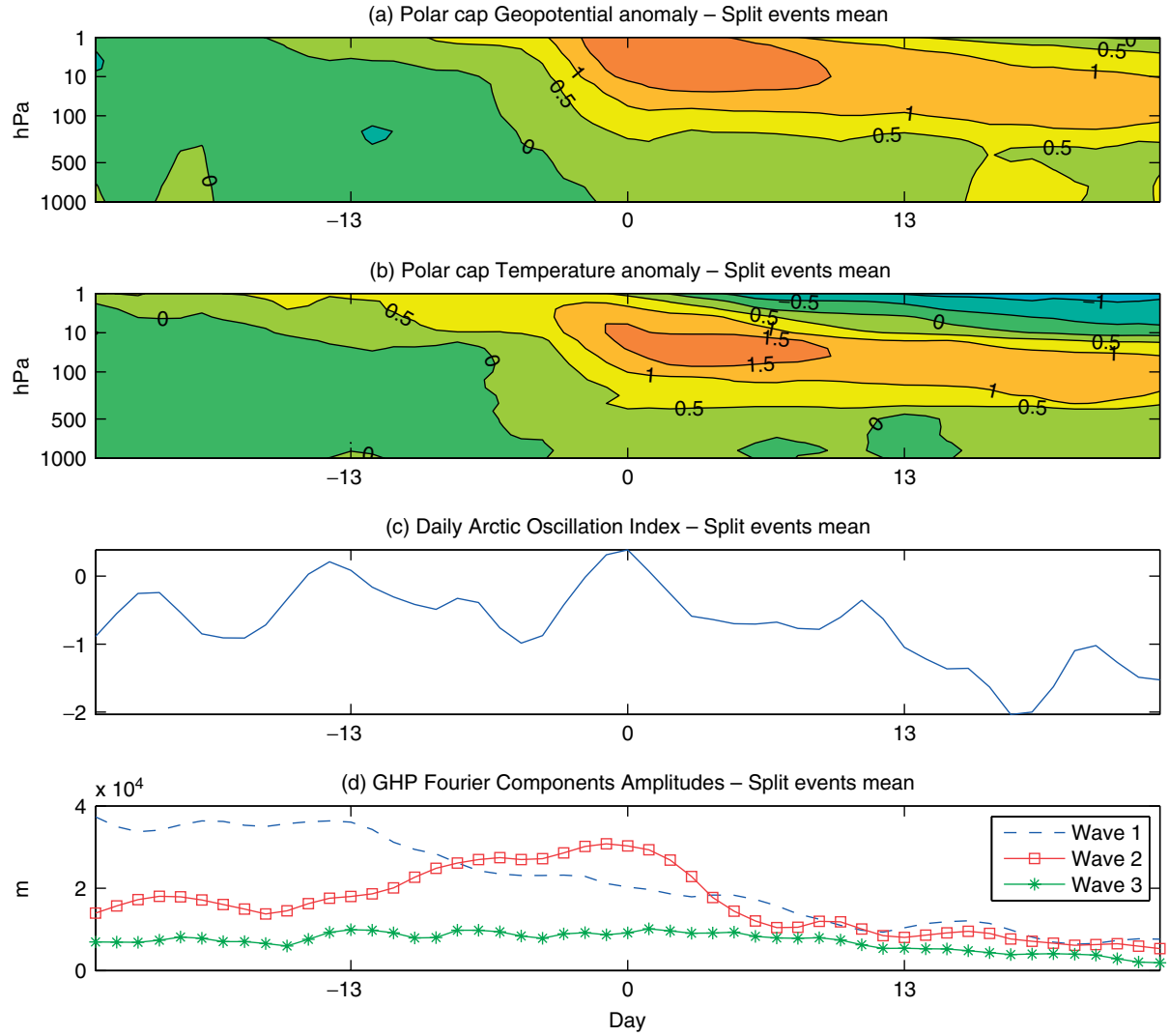

Figure 6. Averages over the 1979–2009 split events of: (a) Normalized 1000–1 hPa geopotential height anomaly with respect to its climatological average (1989–2009), averaged poleward of 60°N; (b) is as (a), but for the temperature anomaly; (c) daily mean AOI; (d) 10 hPa 30–60°N averaged geopotential height wave components: 1 (dashed line), 2 (line with squares) and 3 (line with asterisks). All the time series are plotted over the interval (–25, +25) days around the central date. This figure is available in colour online at wileyonlinelibrary.com/journal/qj

split events during the ERA-40 years, that blocking synoptic configurations usually follow (and/or precede) SSW splitting events. Since synoptic wave activity acts as a main driver for the maintenance of these configurations, its observed increase following SSWs could be responsible for the geopotential anomaly persistence in the lower troposphere, leading to a feasible amplification mechanism of the tropospheric response.

6. Conclusions

In the present study we have pointed out some remarkable facts connected with the occurrence of the February 2010 AOI extreme negative value:

(i) the precondition of a negative AOI at the beginning of January, primarily associated with a minor SSW event which occurred during December 2009;
(ii) the rapid succession of two polar vortex splits, where the first one opened the way for the amplification effect of the geopotential anomaly produced by the second one;
(iii) the role of the wavenumber-3 component of the Rossby wave propagating into the stratosphere, causing the breaking of the polar vortex into three separate patches, clearly distinguishable in the vorticity content;
(iv) the observed increase of the baroclinic activity at middle latitudes, causing the enhancement of meridional mass and energy exchanges.

While each of these facts is in a sense unique with respect to the observed past SSW events, due to the nonlinearity of the dynamics, it is very hard to assess which one actually led to the AOI extreme value. In our opinion, only the combination of these factors, intimately connected with each other, is able to explain the registered historical record.

In conclusion, we note that in a normally occurring SSW event, no (or just a single) polar vortex breaking event occurs (depending on whether the forcing is of wave-1 or wave-2 type). In the present case, an unusually rapid sequence of two polar vortex breaking events, following a major SSW, took place. After the wave-1 and the wave-2 forcing, determining the first polar vortex split, a new wave-3 forcing appeared, which caused a further splitting into three separate centres.

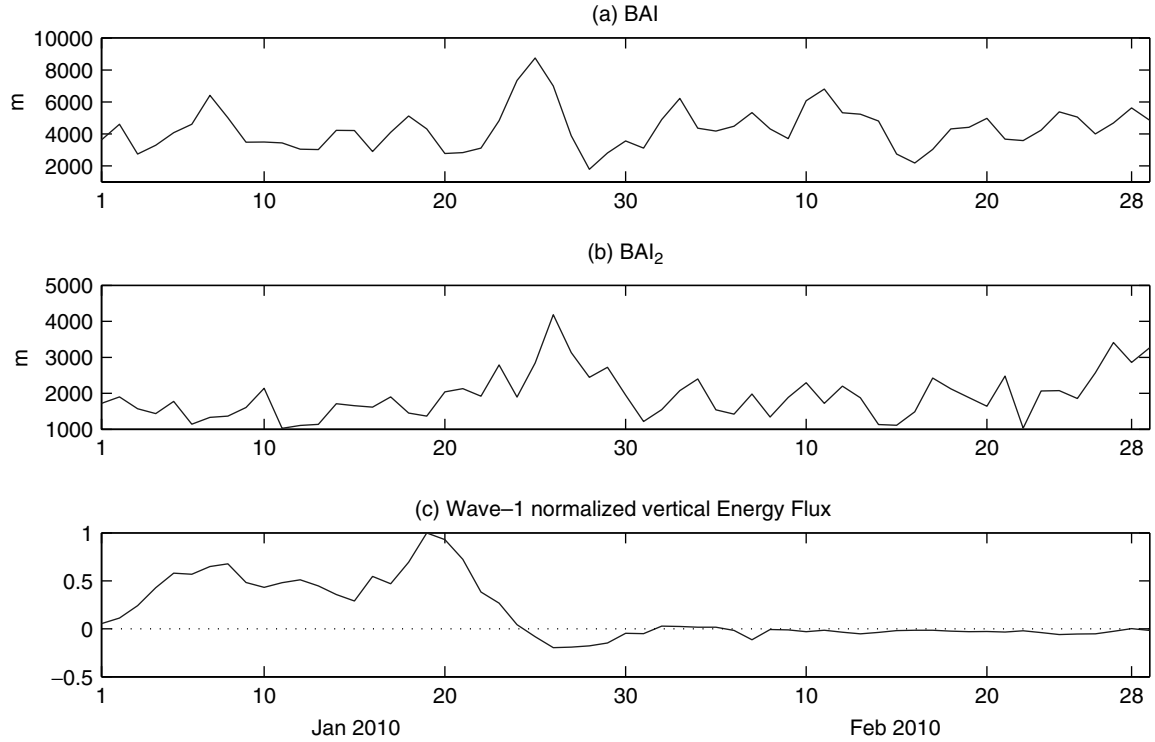

Figure 7. Time series of Baroclinic Activity Index (m) calculated for (a) the wave components 6, 7, 8 (BAI), and (b) the wave components 9, 10, 11 (BAI_2). (c) shows the normalized wave-1 vertical energy flux, averaged over the latitudinal band 30–85°N at 10 hPa.

Finally, investigation of the possible physical mechanisms underlying (i) the energy transfer from the stratosphere to the troposphere, and (ii) the connection between anomalous baroclinic activity and the AO response, will be the subject of future work.

Acknowledgements

We thank the anonymous referees for their critical comments which helped us to improve the content of the paper. Helpful comments on the draft by Ms Charlotte Launtry and Ms Teresa Greco are also kindly acknowledged.

References

Andrews D, Holton J, Leovy C. 1987. *Middle Atmosphere Dynamics.* Academic Press: New York.

Baldwin MP, Dunkerton TJ. 1999. Propagation of the Arctic Oscillation from the stratosphere to the troposphere. *J. Geophys. Res.* **104**: 30937–30946.

Baldwin MP, Dunkerton TJ. 2001. Stratospheric harbingers of anomalous weather regimes. *Science* **244**: 581–584.

Benzi R, Malguzzi P, Speranza A, Sutera A. 1986. The statistical properties of general atmospheric circulation. Observational evidence and a minimal theory of bimodality. *Q. J. R. Meteorol. Soc.* **112**: 661–674.

Blackmon ML. 1976. A climatological spectral study of the 500 mb geopotential height of the Northern Hemisphere. *J. Atmos. Sci.* **33**: 1607–1623.

Charlton AJ, Polvani LM. 2007. A new look at stratospheric sudden warmings. Part I: Climatology and modeling benchmarks. *J. Climate* **20**: 449–469.

Charney JG, Drazin PG. 1961. Propagation of planetary scale disturbances from the lower into the upper atmosphere. *J. Geophys. Res.* **66**: 83–110.

Christiansen B. 2001. Downward propagation of zonal mean zonal wind anomalies from the stratosphere to the troposphere: Model and reanalysis. *J. Geophys. Res.* **106**: 307–322.

Cohen J, Foster J, Barlow M, Saito K, Jones J. 2010. Winter 2009–2010: A case study of an extreme Arctic Oscillation event. *Geophys. Res. Lett.* **37**: L17707.

Coy L, Eckermann S, Hoppel K. 2009. Planetary wave breaking and tropospheric forcing as seen in the stratospheric sudden warming of 2006. *J. Atmos. Sci.* **66**: 495–507.

Eliassen A, Palm E. 1961. On the tranfer of energy in stationary mountain waves. *Geofys. Publ.* **22**: 1–23.

Hannachi A, Mitchell D, Gray L, Charlton-Perez A. 2011. On the use of geometric moments to examine the continuum of sudden stratospheric warmings. *J. Atmos. Sci.* **68**: 657–674.

Hansen AR, Sutera A. 1986. On the probability density distribution of planetary-scale atmospheric wave amplitude. *J. Atmos. Sci.* **43**: 3250–3265.

Harley DE, Villarin JT, Black RX, Davis CA. 1998. A new perspective on the dynamical link between the stratosphere and troposphere. *Nature* **391**: 471–473.

Limpasuvan V, Thompson DWJ, Hartmann DL. 2004. The life cycle of the Northern Hemisphere sudden stratospheric warmings. *J. Climate* **17**: 2584–2596.

Martius O, Polvani LM, Davies HC. 2009. Blocking precursors to stratospheric sudden warming events. *Geophys. Res. Lett.* **36**: L14806.

Matsuno T. 1970. Vertical propagation of stationary planetary waves in the winter Northern Hemisphere. *J. Atmos. Sci.* **27**: 871–883.

Matsuno T. 1971. A dynamical model of stratospheric warmings. *J. Atmos. Sci.* **28**: 1479–1494.

Nakagawa KI, Yamazaki K. 2006. What kind of stratospheric sudden warming propagates to the troposphere? *Geophys. Res. Lett.* **33**: L04801.

Palmer TN. 1982. Properties of the Eliassen–Palm flux for planetary-scale motions. *J. Atmos. Sci.* **39**: 992–997.

Perlwitz J, Harnik N. 2003. Observational evidence of a stratospheric influence on the troposphere by planetary wave reflection. *J. Climate* **16**: 3011–3026.

Polvani LM, Kushner P. 2002. Tropospheric response to stratospheric perturbations in a relatively simple GCM. *Geophys. Res. Lett.* **29**: 1114.

Robinson DA, Dewey F, Heim R Jr. 1993. Northern Hemispheric snow cover: An update. *Bull. Am. Meteorol. Soc.* **74**: 1689–1696.

Simpson IR, Blackburn M, Haigh JD. 2009. The role of eddies in driving the tropospheric response to stratospheric heating perturbations. *J. Atmos. Sci.* **66**: 1347–1365.

Speranza A. 1983. Deterministic and statistical properties of the westerlies. *Paleogeophys.* **121**: 512–562.

Tanaka HL, Tokinaga H. 2002. Baroclinic instability in high latitudes induced by polar vortex: A connection to the Arctic Oscillation. *J. Atmos. Sci.* **59**: 69–82.

Thompson DWJ, Wallace JM. 1998. The Arctic Oscillation signature in the wintertime geopotential height and temperature fields. *Geophys. Res. Lett.* **25**: 1297–1301.
Vitolo R, Ruti PM, Dell'Aquila A, Felici M, Lucarini V, Speranza A. 2009. Accessing extremes of midlatitudinal wave activity: methodology and application. *Tellus* **61A**: 35–49.
Wang L, Chen W. 2010. Downward Arctic Oscillation signal associated with moderate weak stratospheric polar vortex and the cold December 2009. *Geophys. Res. Lett.* **37**: L09707.
Wittman MAH, Charlton AJ, Polvani LM. 2007. The effect of lower stratospheric shear on baroclinic instability. *J. Atmos. Sci.* **64**: 479–496.

